

## **Pitting and Crevice Corrosion Resistance of a Direct Metal Laser Sintered (DMLS) 316L Stainless Steel in Artificial Seawater**

Claudia Prieto, Marc Singer, David Young

Institute for Corrosion and Multiphase Technology  
Department of Chemical and Biomolecular Engineering  
Ohio University, Athens, OH 45701

### **ABSTRACT**

The use of 2%-Mo containing austenitic stainless steels is a common practice for marine applications, such as for the fabrication of fuel nozzles and impellers. Such geometrically complex parts can be manufactured more efficiently using additive manufacturing techniques, such as the direct metal laser sintering process (DMLS). However, research has revealed that 316-type stainless steels are not entirely exempt from undergoing localized attack. Environmental factors, such as chloride content, temperature and oxygen levels are key governing factors limiting the application of 2%-Mo containing austenitic stainless steels. Moreover, the susceptibility to localized attack for additively-manufactured products, such as 316L DMLS, has been postulated to significantly increase due to residual porosity, surface asperity and microstructural defects inherent to the additive manufacturing process. Since the additive manufacturing of geometrically complex parts confers advantages in terms of design, it is essential to determine if their performance against corrosion would compromise their real world applicability. By using aerated artificial seawater per ASTM D1141 and cyclic potentiodynamic polarization (CPP), the metastable pitting characteristics of a 316L stainless steel manufactured by the DMLS process was characterized. Moreover, the effect of an argon quenched heat treatment was explored. A cold-rolled 316L stainless steel, as-received and heat-treated, was used as a reference for this study. Results indicated that the heat treatment increased the pitting resistance initiation of the 316L stainless steel made by DMLS as inherent microstructural defects were healed.

## INTRODUCTION

Selective laser melting is an additive manufacturing (AM) process capable of making geometrically complex metallic parts utilizing computer-aided design (CAD) programs<sup>1,2</sup>. The basic principle is the use of a 'layer-by-layer' forming approach, with powdered metal sintered using powder bed fusion methods (PBF)<sup>1,3</sup>. The direct metal laser sintering (DMLS) technique uses a laser to increase the temperature of the metal powder and induce sintering<sup>1,4</sup>.

DMLS, as well as other AM processes, has the advantage of precision in manufacturing<sup>1-3</sup>, which can make it attractive for marine and biomedical applications. Among stainless steels, low carbon 300-series alloys are typical for this type of manufacturing process<sup>1,3,5-7</sup>; with 316L stainless steel (UNS S31603) the most commonly used<sup>1,3,5-7</sup>. One significant advantage of 316L stainless steel is its resistance to pitting due to the presence of molybdenum (Mo).<sup>8</sup> Consequently, this resistance to corrosion is a crucial factor for potential application of products manufactured as DMLS 316L stainless steel. As a general rule, AM relies on stainless steel to avoid corrosion issues.<sup>1,7</sup> Nonetheless, the corrosion resistance of DMLS 316L stainless steel cannot be assumed. The inherent defects of the parts due to the manufacturing process need to be considered. Porosity, microscopic surface defects (scan tracks and melting pools) and dendritic microstructure can be present in the final product<sup>1-4,9</sup>, and play a significant role in corrosion resistance. Therefore, the current research is focused on assessing the pitting and crevice corrosion resistance of a DMLS 316L stainless steel in artificial seawater.

## EXPERIMENTAL PROCEDURE

### Electrochemical Measurements

The experimental apparatus was a typical 3-electrode setup in a 2L glass cell, as shown in Figure 1. The 316L stainless steel cold-rolled specimens were used as working electrodes. The specimens were cut to squares with a working area of 1 cm<sup>2</sup>. The 316L DMLS specimens were manufactured with a 400 W laser at a volume rate of 2 mm<sup>3</sup>/s, a spot size of 50 µm of radius, and a layer thickness of 20 µm. Samples were flush-mounted in epoxy and lacquer was used on the interface between edges to avoid crevice initiation.<sup>10,11</sup> Table 1 shows the chemical composition of the specimens tested.

**Table 1**

**Chemical composition (wt.%) of the 316L SS samples (as-rolled and DMLS)**

	Al	C	Cr	Cu	Mn	Mo	N	Nb	Ni	P	S	Si	Ti	W	Fe
<b>Rolled</b>	0.011	0.01	16.96	0.41	1.23	2.02	0.04	0.014	10.22	0.032	0.006	0.36	0.013	0.05	balance
<b>DMLS</b>	0.007	0.007	17.61	0.21	1.64	2.68	0.07	0.01	12.1	0.017	0.008	0.26	0.035	0.024	balance

The steel specimens were sequentially polished with 150, 400, and 600 grit silicon carbide paper. They were then rinsed with isopropanol and sonicated for 5 minutes to remove any debris from polishing. A platinum-coated titanium mesh was used as the counter

electrode. A saturated Ag/AgCl electrode was used as the reference electrode connected *via* a Luggin capillary. The working electrolyte was an artificial seawater brine<sup>12</sup> with the composition shown in Table 2.

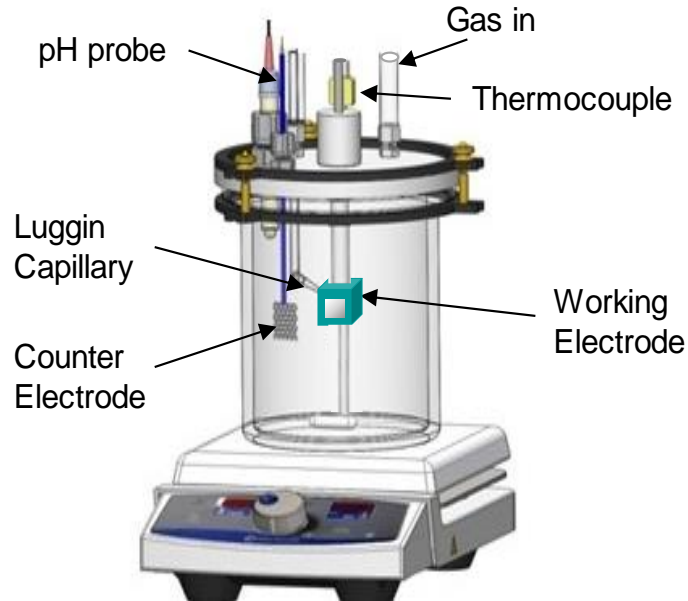


**Figure 1: Three electrode glass cell setup to perform electrochemical measurements**

**Table 2  
Artificial seawater composition**

Compound	Concentration, g/L
NaCl	24.53
MgCl <sub>2</sub>	5.2
Na <sub>2</sub> SO <sub>4</sub>	4.09
CaCl <sub>2</sub>	1.16
KCl	0.695
NaHCO <sub>3</sub>	0.201
KBr	0.101
H <sub>3</sub> BO <sub>3</sub>	0.027
SrCl <sub>2</sub>	0.025
NaF	0.003

Before each experiment, the working solution was deoxygenated by sparging with nitrogen for 2 hours, pH was then adjusted to 8.2 with the addition of a solution of 0.1 M NaOH. After specimen immersion, the open circuit potential (OCP) was monitored for one hour. Cyclic potentiodynamic polarization<sup>10</sup> was performed starting from -100 mV with respect to the OCP at a forward and backward scan rate of 0.166 mV/s, 50 A/m<sup>2</sup> (5

mA/cm<sup>2</sup>) was the apex current set to start the reverse scan. Each experiment was repeated three times.

### **Heat Treatment**

Selected specimens were solution annealed in an argon atmosphere to study the effect of scan tracks<sup>1-4,9</sup>, which are microstructural defects inherent to the DMLS process. Table 3 shows the conditions of the heat treatment.

**Table 3**  
**Heat treatment for annealing**

<b>Heat Treatment</b>	<b>Conditions</b>
Annealing in an argon atmosphere	1100°C Soaking time: 45 min Argon quenched

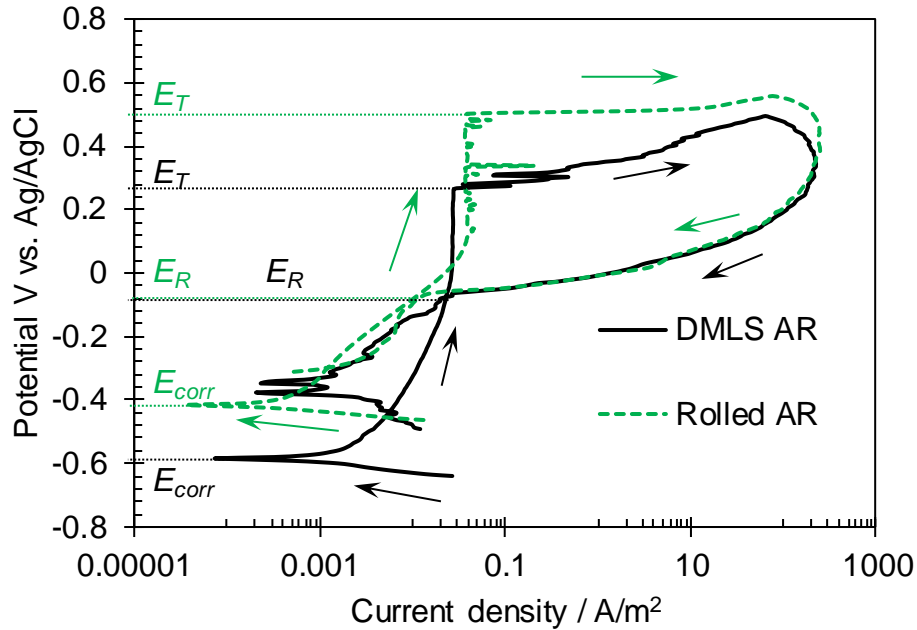
### **Surface Characterization**

SEM was used to characterize the crevices and pitting after the electrochemical experiments. Electron backscatter diffraction (EBSD) was performed to determine the effect of heat treatment on the grain size<sup>13</sup>. The samples were sequentially polished with 150, 400, and 600 grit silicon carbide abrasive paper. After that, the specimens were polished with 9, 6, 3, and 1 μm diamond suspension. For EBSD, the polishing continued with 0.05 μm alumina suspension then electropolishing was performed to remove the Beilby layer and enhance map acquisition<sup>14</sup>.

## **RESULTS AND DISCUSSION**

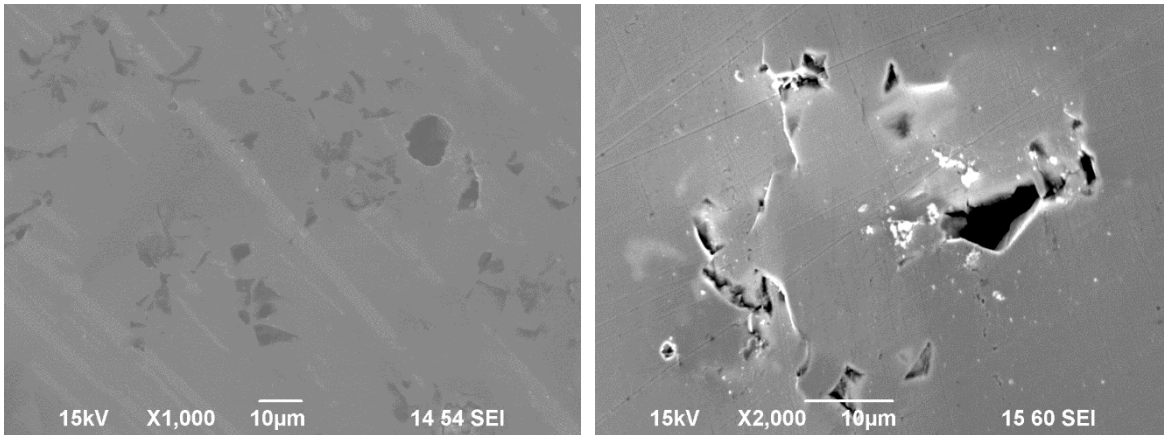
### **Corrosion Test**

Figure 2 shows the cyclic potentiodynamic polarization of the 316L cold-rolled and DMLS as-received specimens. Initially, it was observed that the corrosion potential ( $E_{corr}$ ) of the DMLS was, on average, 183 mV lower (standard deviation of 12.2 mV) than its cold-rolled counterpart. It was also observed that the transpassivation potential ( $E_T$ ) of the DMLS was reduced by 194 mV on average (standard deviation of 5.7 mV), whereas the repassivation potential was virtually the same with an average difference of 18 mV.



**Figure 2. Cyclic potentiodynamic polarization curves for the DMLS and cold-rolled 316L SS.  $E_{corr}$  is the corrosion potential;  $E_T$  is the transpassivation potential, and  $E_R$  is the repassivation potential.**

Another substantial difference between the materials was found after the test. The pitting and crevice morphology for both specimen types was characterized by SEM as shown in Figure 3 and Figure 4. Figure 3 shows the pits found after the electrochemical measurements of the 316L cold-rolled as-received specimen.



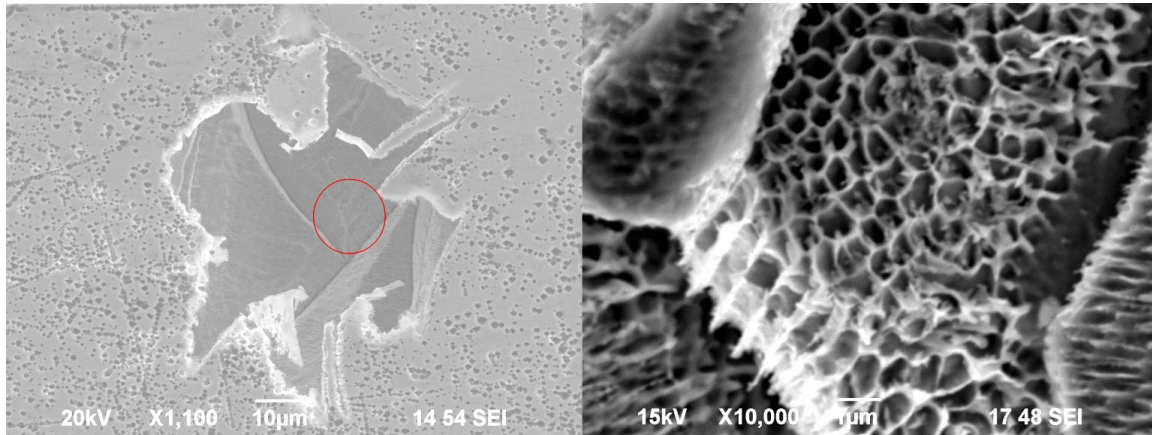
**Figure 3. Pitting morphology of the 316L cold-rolled as-received specimens after the cyclic potentiodynamic polarization test.**

Figure 4 shows the crevice morphology of the 316L DMLS as-received specimen after the cyclic potentiodynamic polarization. The main difference between the damage of the

surface during the test of the 316L cold-rolled and the 316L DMLS is the size of the pits. Otero, *et al.*, have described this mode of attack as crevice corrosion in stainless steels manufactured by powder metallurgy<sup>15</sup>. The authors described that the corrosion initiates in pores due to hydrolysis caused by the water therein, as shown by Equation (1).



Such a reaction produces hydrogen ions, thereby lowering the local pH. The difference between the local chemistry at the interior of the pore and the surface metal causes crevice corrosion<sup>15</sup>.



**Figure 4. SEM images showing a crevice after the cyclic potentiodynamic polarization test. A zoom image of the red circle showed the presence of dendritic structure for the 316L SS DMLS.**

It is noteworthy that the main distinction between the cold-rolled and the DMLS stainless steel specimens lies in the dendritic structure that is exposed after the test. A similar dendritic structure with this material was found from previous researchers in additively manufactured stainless steels<sup>16,17</sup>. The chemical segregation of alloying elements, such as molybdenum in the microstructure, was associated with the preferential corrosion initiation of this type of steel<sup>16,17</sup>.

Similarly to previous research<sup>16</sup>, a heat treatment was performed to reduce superficial defects (scan tracks). As a result, the cyclic polarization curve for the heat treated material (Figure 5) showed a slight improvement in terms of transpassivation potential as it increased an average of  $118 \pm 15$  mV. Also, the repassivation potential decreased by an average of  $35 \pm 5$  mV.

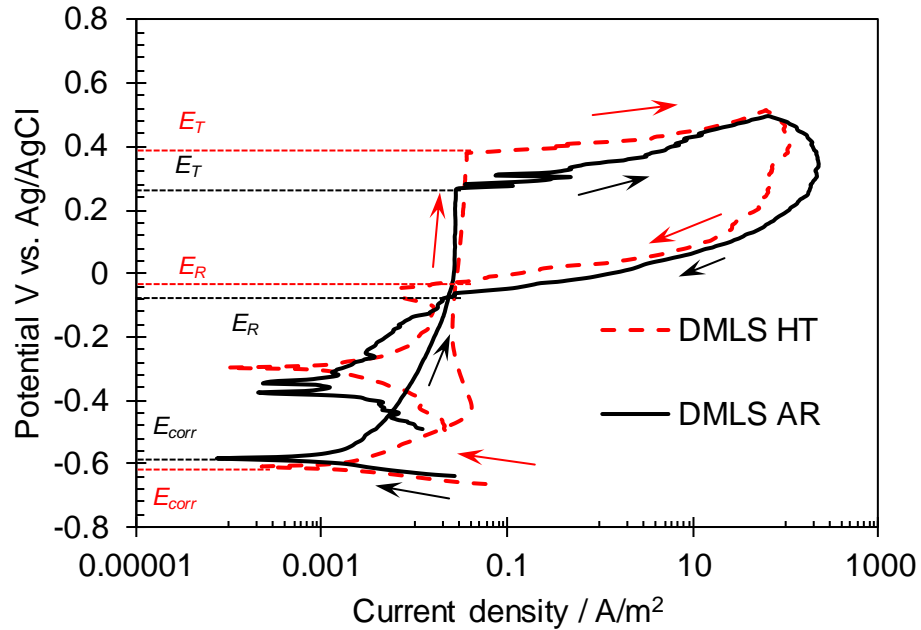


**Figure 5. Cyclic potentiodynamic polarization curves for the DMLS as received and DMLS after heat treatment.  $E_{corr}$  is the corrosion potential;  $E_T$  is the transpassivation potential, and  $E_R$  is the repassivation potential.**

For comparison purposes, the as rolled material was subjected to the same heat treatment as the DMLS specimens. Cyclic polarization curves were obtained as shown in Figure 6. The main difference in the curve, before and after the heat treatment, is the open circuit potential ( $E_{corr}$ ) which increased  $183 \pm 20$  mV. Regarding the transpassivation potential ( $E_T$ ), the changes were insignificant as the heat-treated material exhibited a transpassivation potential  $25 \pm 7$  mV lower than the as-received. Finally, the repassivation potential ( $E_R$ ) increased by  $88 \pm 12$  mV.

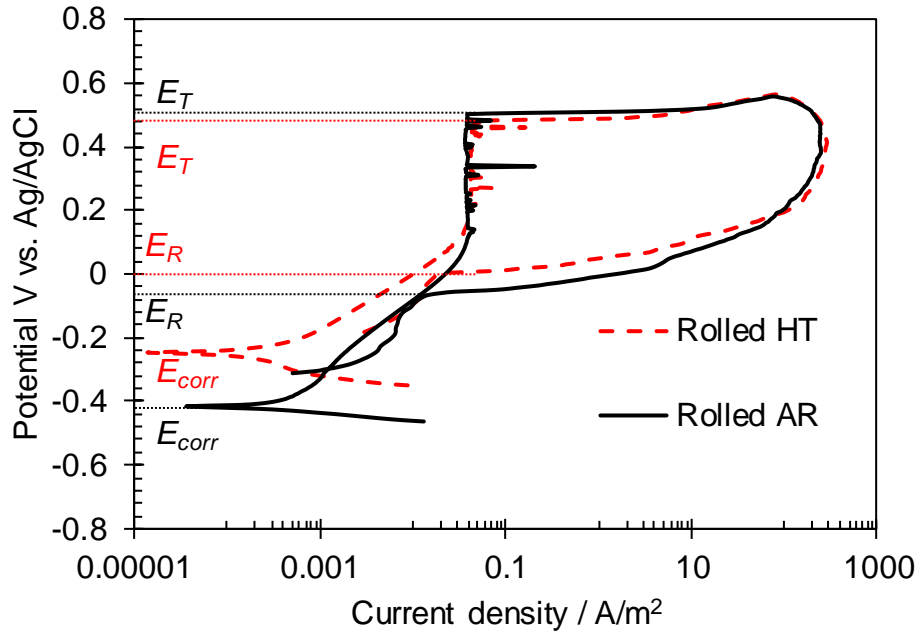


**Figure 6. Cyclic potentiodynamic polarization curves for the as Rolled as received and Rolled after heat treatment.  $E_{corr}$  is the corrosion potential;  $E_T$  is the transpassivation potential, and  $E_R$  is the repassivation potential.**

Finally, both DMLS and rolled heat-treated specimens were compared as shown in Figure 7. The open circuit potential difference from both curves was  $395 \pm 40$  mV. On the other hand, the transpassivation potential difference was  $76 \pm 8$  mV. Finally, the repassivation potential differed by  $37 \pm 8$  mV. Comparing to the anodic behavior of the materials before the heat treatment (Figure 2), the transpassivation potential difference was diminished.

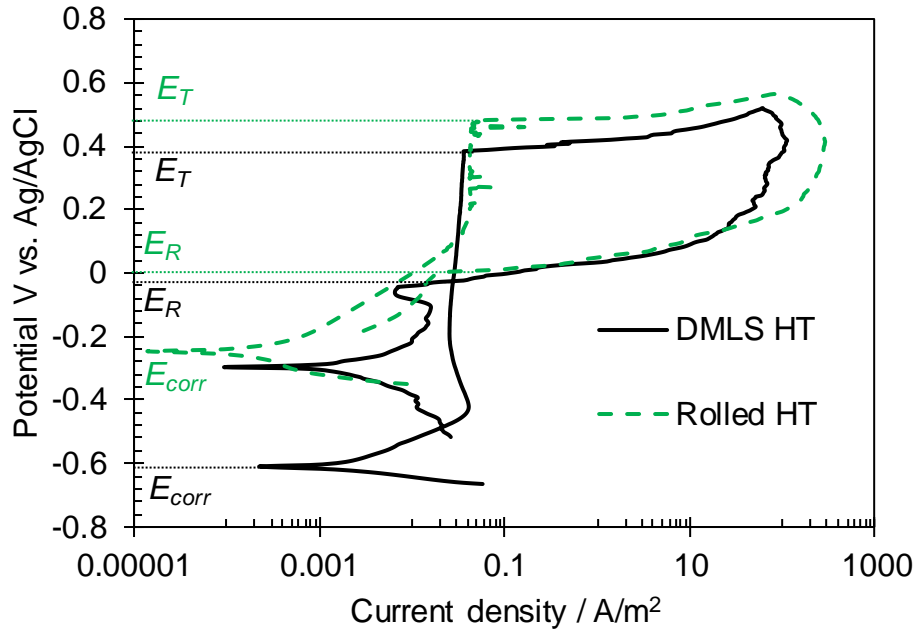


**Figure 7. Cyclic potentiodynamic polarization curves for the as-rolled and DMLS specimens after heat treatment.  $E_{corr}$  is the corrosion potential;  $E_T$  is the transpassivation potential, and  $E_R$  is the repassivation potential.**

Additionally, the pit morphology after the test did not show the dendritic structure observed in the previous experiment for the as-received DMLS specimen, as illustrated by Figure 8.

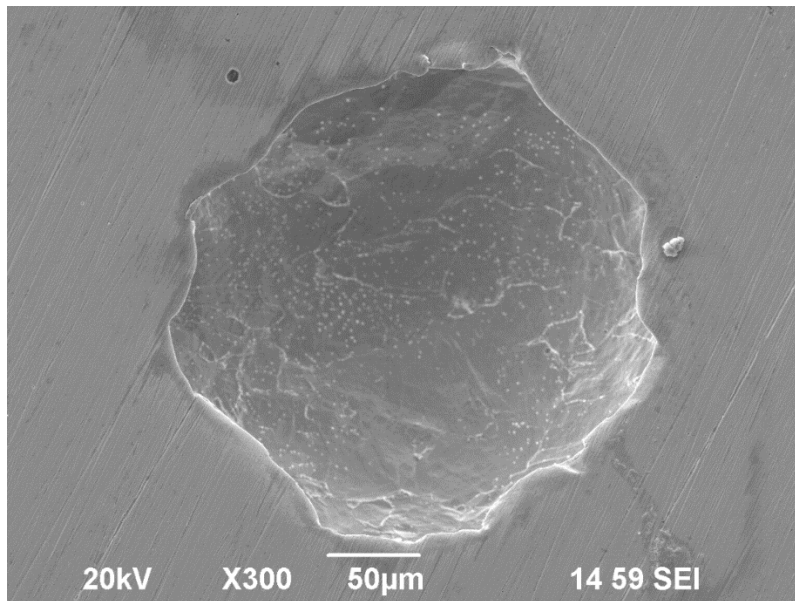
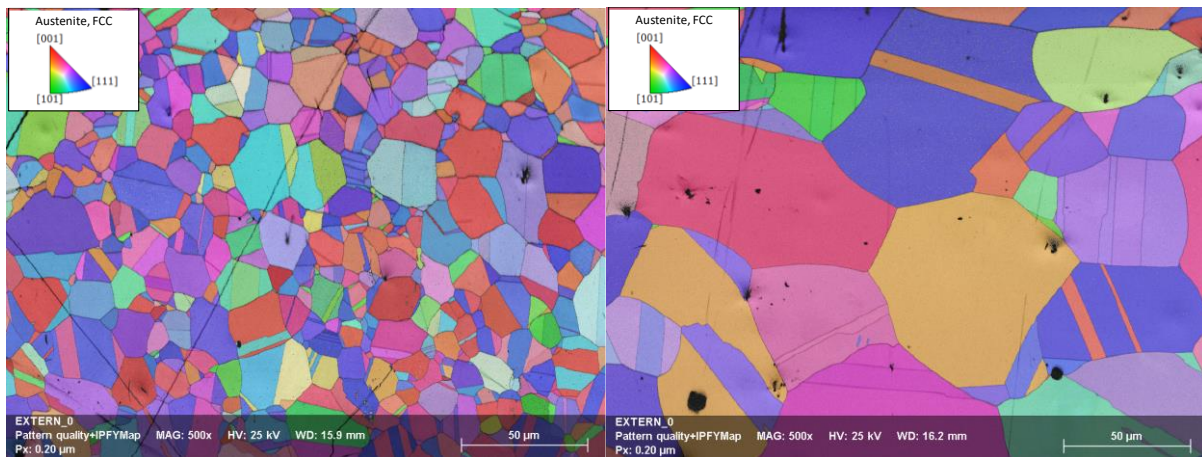


**Figure 8. SEM image showing a pit after the polarization test of a 316L DMLS heat treated. No dendritic structure was found inside the pit.**

## EBSD Analysis

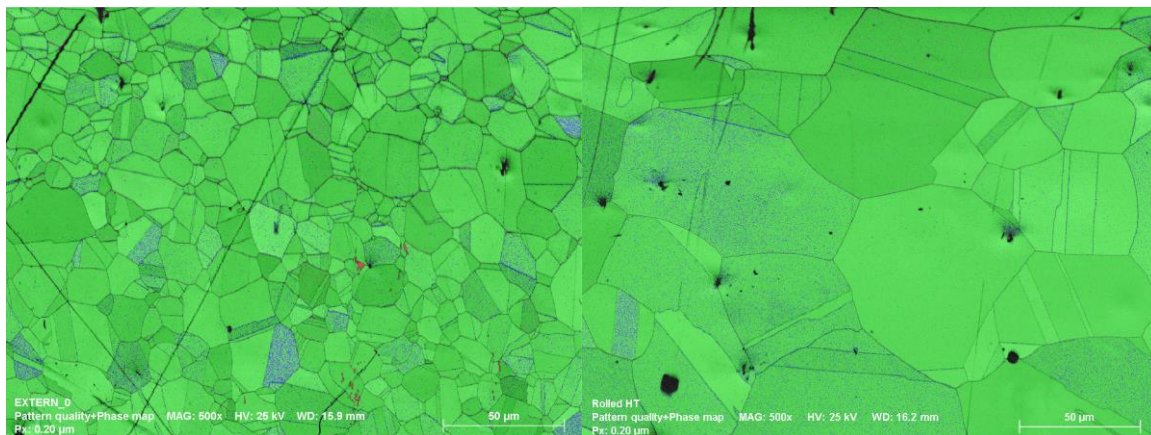
Since there was an improvement in the passivation potential due to the heat treatment mainly associated with the healing of surface defects, EBSD was utilized to explore if the heat treatment caused a change in the phase composition of the stainless steel.

Figure 9 shows the EBSD analysis of the cold-rolled 316L stainless steel as-received and after heat treatment. The phase distribution analysis indicated that austenite was the primary phase in both cases. Regarding the grain size analysis for the as-received specimen, it was observed to have equiaxed grains with an average diameter of  $15 \pm 2 \mu\text{m}$ . After heat treatment, the average grain diameter increased to  $45 \pm 7 \mu\text{m}$ .



**Figure 9. EBSD orientation map for the cold-rolled 316L SS as received (left) and heat-treated (right)**

Figure 10 shows the phase map for the 316L stainless steel specimens before and after the heat treatment.



**Figure 10. EBSD phase map for the cold-rolled 316L SS as received (left) and heat-treated (right). Light green: austenite; red: ferrite; blue: chromium carbide.**

A quantitative analysis of secondary phases was performed on both specimens. The percentage of phases is given by Table 4. EDS analysis in conjunction with EBSD software (chemical composition and stoichiometry in conjunction with crystallography) was able to identify more than 96% of the phases present in the mapping analysis. As a result of the heat treatment, the percentage of austenite increased by 2%; the initial ferrite content of the cold-rolled as-received decreased by one order of magnitude; finally, chromium carbide ( $\text{Cr}_{23}\text{C}_6$ ) increased by 0.5%. The presence of chromium carbide can cause a deleterious effect on the corrosion resistance of stainless steels<sup>18</sup>.

**Table 4**

**Phase mapping quantitative analysis for 316L cold-rolled AR and HT**

<b>Phase</b>	<b>As Received</b>	<b>Heat Treated</b>
Austenite	92.3	94.3
Ferrite	0.146	0.069
Chromium Carbide ( $\text{Cr}_{23}\text{C}_6$ )	3.64	4.18
Other (no solution)	3.6	1.52

Regarding the DMLS specimens, the EBSD phase mapping analysis shown in Figure 11, indicated that austenite was the primary phase. For this type of specimen, there were elongated grains before and after performing heat treatment, with austenite as the main phase in both cases. For the DMLS, the heat treatment was not sufficient to promote recrystallization of elongated grains into equiaxed grains as reported in other researches<sup>19,20</sup>. A similar phenomenon was reported by Kong, *et al.*<sup>20</sup> The author reported that recrystallization of elongated grains not always occurred during the heat treatment<sup>20</sup>.

A possible explanation for not having recrystallization is given by Laasraoui and Jonas<sup>21</sup>. The authors explained that the recrystallization of austenitic grains is promoted by the presence of dislocations and strain in the grains<sup>21</sup>. The higher the strain/dislocations, the higher the stored energy. The stored energy is the driving force for recrystallization<sup>21</sup>. In the case of the DMLS, since the process involves sintering the powder rather than melting it, there are few strain and dislocations<sup>22</sup>. This condition produces poor recrystallization<sup>21</sup>.

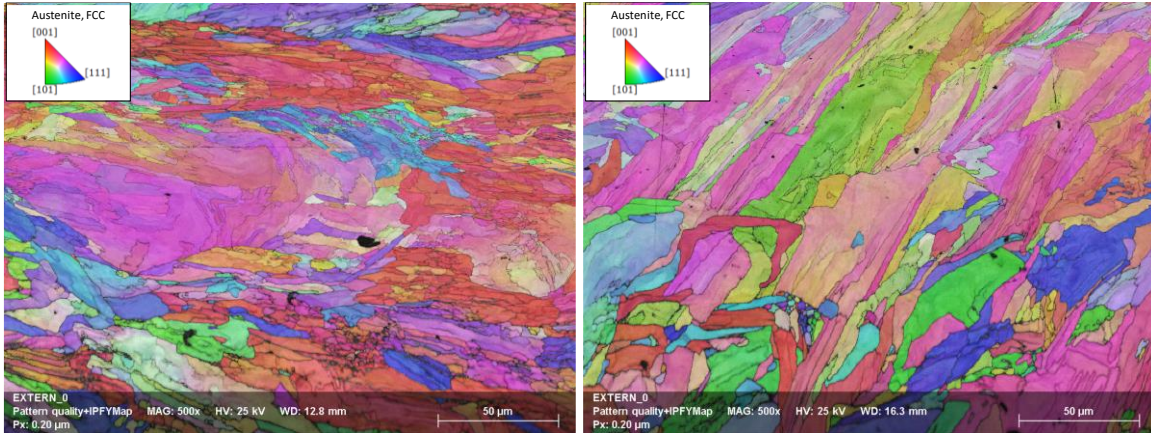


**Figure 12. EBSD orientation map for the DMLS 316L SS as received (left) and heat-treated (right)**

Similar to the 316L cold-rolled, a quantitative analysis was also performed in the DMLS 316L SS to identify and quantify secondary phases in the as-received and heat-treated specimens. Figure 13 shows the phase map of both specimens. Table 5 shows the quantification of the phase distribution. Results indicated that the heat treatment had a similar effect than the cold-rolled counterpart. The content of austenite increased almost 1% and the ferrite content decreased by one order of magnitude. For the presence of chromium carbides, results showed an increase from 3.3 to 5.4%.

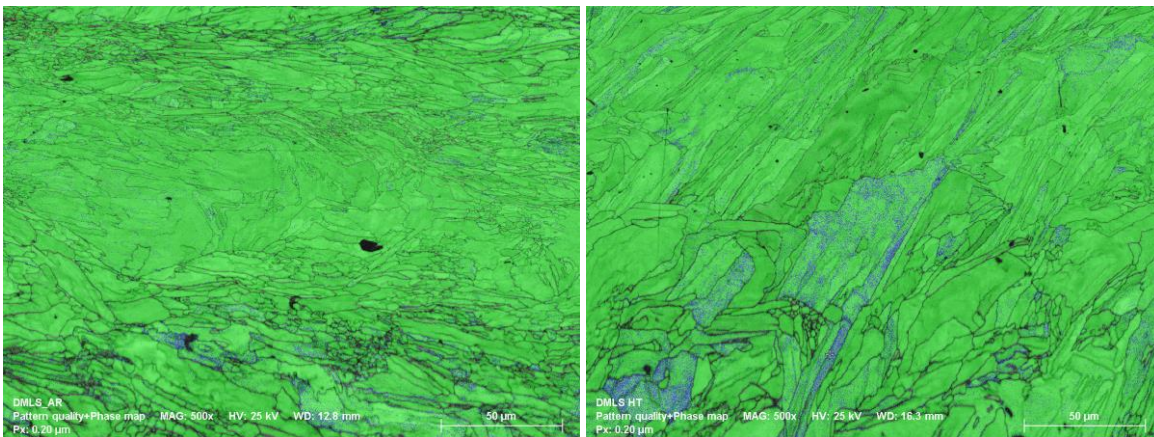


**Figure 13. EBSD phase map for the cold-rolled 316L SS as received (left) and heat-treated (right). Light green: austenite; red: ferrite; blue: chromium carbide.**

**Table 5**

**Phase mapping quantitative analysis for 316L DMLS AR and HT**

Phase	As Received	Heat Treated
Austenite	87.4	88.5
Ferrite	0.191	0.088
Chromium Carbide (Cr <sub>23</sub> C <sub>6</sub> )	3.31	5.43
Other (no solution)	9.1	5.94

These results suggest that the beneficial effect of heat treatment on the pitting resistance of a 316L DMLS stainless steel is only associated with healing superficial defects on the steel, making it less susceptible to initiation of localized corrosion. On the other hand, the side effect of heat treatment was the increase of secondary phases such as chromium carbides. Such effects need to be addressed in future work.

## CONCLUSIONS

- The superficial microstructural defects of a 316L stainless steel manufactured by the direct metal laser sintering (DMLS) process have a deleterious effect on the localized corrosion resistance of the stainless steel.
- By healing the defects *via* heat treatment, the localized corrosion resistance was improved in terms of pitting potential and pitting morphology (healing the dendritic structure). However, the increase of deleterious phases in the steel as a result of the heat treatment, such as chromium carbides, needs to be considered for practical application.

## ACKNOWLEDGMENTS

The authors would like to thank GPI Prototype and Manufacturing Services and Dr. T.J. Cyders from the Department of Mechanical Engineering, Ohio University for supplying the specimens utilized in the test.

The author expresses her gratitude to Mr. Dan Satko, from Material Resources LLC, Beavercreek, OH, for electropolishing the metal samples for EBSD testing.

## REFERENCES

1. I., Gibson, Rosen, and B. Stucker, *Additive Manufacturing Technologies*, 1<sup>st</sup> ed. (New York, NY: Springer, 2010), pp. 1-42
2. J. P. Kruth, P. Mercelis, J. Van, V. L. Froyen, M. Rombouts, J. Van Vaerenbergh, and L. Froyen, "Binding mechanisms in selective laser sintering and selective laser melting," *Rapid Prototyp. J.*, 11, 5, (2005): pp. 314–326
3. S. S. Panda, V. Singh, A. Upadhyaya, and D. Agrawal, "Sintering response of austenitic (316L) and ferritic (434L) stainless steel consolidated in conventional and microwave furnaces," *Scr. Mater.*, 54, 12, (2006): pp. 2179–2183.
4. A. Simchi, F. Petzoldt, and H. Pohl, "On the development of direct metal laser sintering for rapid tooling," *J. Mater. Process. Technol.*, 141, 3, (2003): pp. 319–328.
5. L.-Å. Norström, "The influence of nitrogen and grain size on yield strength in Type AISI 316L austenitic stainless steel," *Met. Sci.*, 11, 6, (1977): pp. 208–212.
6. S. A. Maloy, M. R. James, G. Willcutt, W. F. Sommer, M. Sokolov, L. L. Snead, M. L. Hamilton, and F. Garner, "The mechanical properties of 316L / 304L stainless steels, Alloy 718 and Mod 9Cr ± 1Mo after irradiation in a spallation environment," *J. Nucl. Mater.*, 296, (2001): pp. 119–128.

7. M. McGuire, *Stainless Steels For Design Engineers*, 1<sup>st</sup> ed. (Materials Park, OH: ASM International, 2008), pp. 69-90.
8. K. Sugimoto and Y. Sawada, "The Role of Molybdenum Additions to Austenitic Stainless Steels in the Inhibition of Pitting in Acid Chloride Solutions," *Corros. Sci.*, 17, (1977): pp. 425–445.
9. R. M. Molak, K. Paradowski, T. Brynk, L. Ciupinski, Z. Pakiela, and K. J. Kurzydowski, "Measurement of mechanical properties in a 316L stainless steel welded joint," *Int. J. Press. Vessel. Pip.*, 86, 1, (2009): pp. 43–47.
10. ASTM G61 (latest revision), "Standard Test Method for Conducting Cyclic Potentiodynamic Polarization Measurements for Localized Corrosion Susceptibility of Iron-, Nickel-, or Cobalt-Based Alloys" (West Conshohocken, PA: ASTM International).
11. G. Sander, S. Thomas, V. Cruz, M. Jurg, N. Birbilis, X. Gao, M. Brameld, and C.R. Hutchinson, "Unexpected Interface Corrosion and Sensitization Susceptibility in Additively Manufactured Austenitic Stainless Steel," *Corrosion*, 74, 2, (2018): pp. 153-157.
12. ASTM D1141 (latest revision), "Standard Practice for the Preparation of Substitute Ocean Water" (West Conshohocken, PA: ASTM International).
13. K.P. Mingard, B. Roebuck, E.G. Bennett, M.G. Gee, H. Nordenstrom, G. Sweetman, and P. Chan, "Comparison of EBSD and conventional methods of grain size measurement of hardmetals," *Int. J. Refract. Met. Hard Mater.* 27 (2009): pp. 213–223.
14. G.L. Wynick and C.J. Boehlert, "Use of electropolishing for enhanced metallic specimen preparation for electron backscatter diffraction analysis," *Mater. Charact.* 55 (2005): pp. 190–202.
15. E. Otero, A. Pardo, M. V. Utrilla, E. Sáenz, and J.F. Álvarez, "Corrosion behaviour of AISI 304L and 316L stainless steels prepared by powder metallurgy in the presence of sulphuric and phosphoric acid," *Corros. Sci.* 40 (1998): pp. 1421–1434.
16. C. Prieto, M. Singer, T. Cyders, and D. Young, "Investigation of pitting corrosion initiation and propagation of a type 316L stainless steel manufactured by the direct metal laser sintering process", *Corrosion* 75, 2, (2019): pp. 140-143.
17. J.R. Trelewicz, G.P. Halada, O.K. Donaldson, and G. Manogharan, "Microstructure and Corrosion Resistance of Laser Additively Manufactured 316L Stainless Steel," *JOM* 68 (2016): pp. 850–859.
18. C.S. Tedmon, D.A. Vermilyea, and J.H. Rosolowski, "Intergranular Corrosion of Austenitic Stainless Steel," *J. Electrochem. Soc.* 118 (1971): pp. 192–202.